1.2.3 Crystal Diffraction Medical Imaging Lens

The first full-scale crystal-diffraction medical-imaging lens has been completed and tested. The lens consists of 13 concentric rings of copper single crystals aligned in such a manner that they all focus gamma rays or x-rays coming from a small source onto a small detector. The lens is capable of focusing x-rays and gamma rays with energies between 80 keV and 250 keV. The latest version of this imaging system is shown in Fig. 1.3. It is clear from this figure that the imaging system does not have to be close to the patient, eliminating any possible claustrophobia effect.

Fig. 1.3. The crystal diffraction medical-imaging lens system. The lens is located in the central cylinder section, the NaI detector is mounted at the upper end, and the breast phantom (with a small radioactive sample located inside) is shown below the end of the imaging system.

Tests of the imaging lens system were performed with energies of 121 keV (^{57}Co) and 141 keV (^{99}Tc), the latter being the most common source in medical imaging. Recent x-ray optics developments have reduced the spatial resolution to 3 mm FWHM (for a 1-mm-diameter source). This resolution is a factor of three better than most of the imaging systems in use today and is as good (and in most cases better) than the PET scanning instruments that are currently being developed.

The crystal-lens imaging system can be applied to small animals (e.g., rabbits, rats, or mice) that are used by the pharmaceutical industry for testing of newly developed drugs. It can also be used to image small parts of the human body such as blood vessels. Based on the data obtained with this lens, we are considering lenses with still better resolution, possibly as small as 1 mm FWHM. This resolution would allow the detection of very small tumors in places such as the female breast or in small test animals. There are many possibilities for nonmedical applications of such a lens system, including the examination of nuclear fuel elements and the location of radioactive material within a larger mass.

1.3 Time-Resolved X-ray Techniques Development

The time-resolved x-ray program can be divided into three parts: radiographic studies of fuel sprays, *in situ* measurements of nanoparticles in polymer-film systems, and x-ray streak camera development. Breakthroughs have been made in each of these areas during the time period covered by this report.

1.3.1 Real-Time Diffusion Dynamics of Polymer/Metal Nanocomposites Using X-ray Standing Waves

Polymer/metal nanocomposites have emerged in recent years as an important research area due to their practical and fundamental significance. Fundamental questions can be addressed by studying individual particle interactions with homopolymers (Shull & Kellock, 1995). In this study, we probed the polymer/metal interactions using a model nanocomposite system. The diffusion of the gold nanoparticles in polymeric thin films was measured in real time as the nanocomposite is annealed above the glass transition temperature (T_g). Total external reflection x-ray standing waves (TER-XSWs) were used to determine the profile of the metal particles perpendicular to the polymer surfaces during slow diffusion dynamics.

Float glass substrates were first placed in a thermal evaporation system and coated with a silver mirror. Poly(tert-butyl acrylate) (PtBA), MW = 352,000 g/mol, thin films (400 Å) were then spun cast from a butanol solution (Cole et al., 1999). The samples were then placed back in the evaporation system, where a thin layer of gold was deposited on the polymer films. The 4 Å gold layer was then sandwiched by another thin polymer film (400 Å) floated from a water bath. X-ray standing wave (XSW) experiments were performed at the 1-BM beamline under a helium environment. The x-rays were monochromatized to an energy of 12.1 keV, optimized for promoting Au L fluorescence.

Previously, the XSW method was used to locate a heavy atom marker layer in thin films with angstrom spatial resolution above a mirror surface (Bedzyk et al., 1989; Wang et al., 1991). The spatial distribution of the gold marker can be obtained by fitting the fluorescence profile as a function of incident angle with a realistic model (Parratt, 1954). The reflectivity and fluorescence experimental data at room temperature along with the fits are shown in Fig. 1.4. The reflectivity and fluorescence data were fitted up to the critical angle of the silver mirror, which is 5.08 mrad, as seen by the sharp decrease in the reflectivity.

The fluorescence yield is a convolution of the electric field intensity and the spatial distribution. In the current work, a Gaussian distribution was assumed with two fitting parameters: the half-width half-max (HWHM) of the distribution and its mean position above the mirror surface. The fit in Fig. 1.4b shows that the gold layer has a HWHM of 16 Å and is situated 366 Å above the mirror surface.

The samples were then annealed above T_g (= 49°C) to allow the gold nanoparticles to diffuse. The fluorescence profile taken after 180 minutes at 85°C is shown in Fig. 1.4c. The fit to the fluorescence profile shows significant broadening (HWHM = 40 Å) of the gold distribution, as well as movement of the mean position towards the air/film interface. This is partially attributed to the asymmetric nature of the mobility of the polymer films, since the silver substrate layer limits motion of the bottom PtBA chains. The HWHM values collected in real time during the anneal were used to determine effective diffusion coefficients that are on the order of 10^{-18} cm^2/s, showing the sensitivity of TER-XSWs to small diffusion distances.

1.3.2 Crystal Optics Simulations for X-ray Free-Electron Laser Pulses

Perfect crystal optics are expected to continue to be important for mono-

chromatizing and manipulating x-ray beams at fourth-generation x-ray sources. Given this, examining the fundamental physics of perfect-crystal diffraction (i.e., dynamical diffraction theory) in the regime of ultrashort (femtosecond) pulses is worthwhile. In this regime, the pulse lengths are comparable to or shorter than the extinction length scales of the crystal reflection. We have developed computer programs to calculate the diffraction properties under ultrashort pulses, initially without consideration of damage due to the high peak fields. Initial work consisted of computation of the Green's functions corresponding to crystal-reflection responses to incident Δ-function electromagnetic impulses in Bragg and Laue geometries, for both reflected and transmitted beams. In addition to demonstrating quantitatively how crystal reflections respond to impulses, these simulations pointed out the effect of delayed echos from back-face diffraction in thin Bragg crystals. (A similar effect exists for Laue crystals.) The studies were taken further to examine the modification of a self-amplified spontaneous emission (SASE) x-ray free-electron laser (XFEL) pulse's temporal structure through single- and double-crystal reflections of low and high orders. In addition to simulating the degree of smearing of an incident pulse's microbunching structure, the shot-to-shot time-integrated intensity fluctuations were examined (Fig. 1.5).

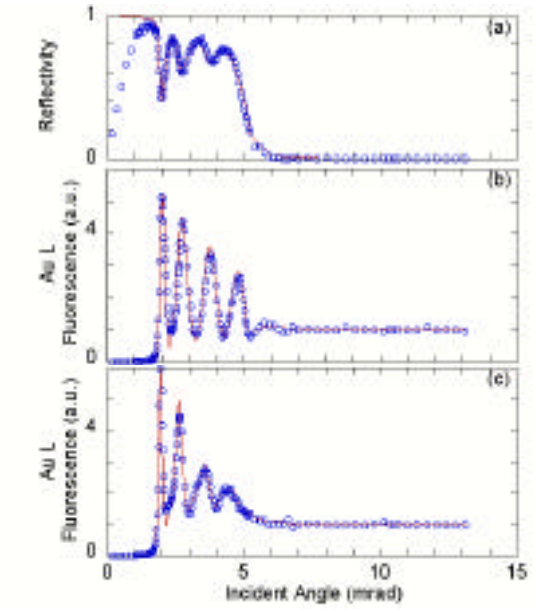

Fig. 1.4. Experimental data (circles) and fits (lines) at room temperature for (a) reflectivity and (b) fluorescence. The fluorescence profile after the sample has been annealed at 85°C for 180 minutes is shown in (c).

Attention has also been directed towards understanding the high-field-induced nonlinear corrections to the elastic-scattering cross section. This was deemed important in light of the possible necessity of modification of the electronic susceptibility for a dynamical diffraction theory valid at high x-ray intensities. Also motivating this issue is the frequently contemplated future technique of single-shot (or few-shot) diffraction studies of materials with focused XFEL beams. It is reasonable to ask whether, at such high intensities, the scattering intensities have the same quantitative interpretation (in connection to electronic structure) as in conventional x-ray scattering. To examine this, the next order perturbative correction to the usual (linear) scattering factor for x-rays was estimated to be 5 orders of magnitude weaker than the Thomson cross section.

1.4 High-Energy X-ray Scattering

The high-energy x-ray program is heavily involved in the development of instrumentation and techniques that will be used on a dedicated high-energy beamline at the APS (the former HEX-CAT project).